*Journal of Biomolecular NMR* **29:** 57–64, 2004.



# Combined frequency- and time-domain NMR spectroscopy. Application to fast protein resonance assignment

Bernhard Brutscher
*Institut de Biologie Structurale – Jean-Pierre Ebel, UMR5075 CNRS-CEA-UJF, 41, rue Jules Horowitz, 38027 Grenoble Cedex, France*

Received 17 September 2003; Accepted 23 November 2003

*Key words:* GFT, Hadamard spectroscopy, protein resonance assignment, reduced dimensionality

**Abstract**

A simple and general method is presented to simplify multi-dimensional NMR spectra of isotope-labeled biomolecules. The approach is based on band-selective Hadamard-type frequency encoding, which disperses the correlation peaks into different sub-spectra. This makes it possible to apply low-dimensionality-based NMR techniques to larger molecular systems. Here we demonstrate the use of band-selective Hadamard frequency labeling for fast protein resonance assignment, based on our recently proposed suite of 2D experiments (Bersch et al., 2003).

## Introduction

Multi-dimensional time-domain Fourier-transform (FT) NMR spectroscopy has proven to be very powerful for the study of bio-molecular systems. A major drawback of FT NMR, however, is the time requirement for recording higher-dimensional correlation experiments, which roughly increases by about two orders of magnitude for each additional dimension. Much effort has been spent recently to develop new acquisition schemes for speeding up NMR correlation experiments. Examples of such approaches are reduced dimensionality or GFT NMR (Szyperski et al., 1993a,b, 1994, 1995, 1996, 1998, 2002; Simorre et al., 1994; Brutscher et al., 1994, 1995a,b, 2002; Ding and Gronenborn, 2002; Kim and Szyperski, 2003, Kozminski and Zhukov, 2003; Bersch et al., 2003), Hadamard spectroscopy (Kupce et al., 2003a,b,c,d; Freeman and Kupce, 2003), the filter diagonalization method (Chen et al., 2000, 2003; Mandelshtam, 2001), or single-scan multi-dimensional NMR (Frydman et al., 2002, 2003). Although these are quite distinct techniques, they have in common that they significantly reduce the acquisition time required to record a 'multi-dimensional' NMR spectrum with decent spectral resolution as compared to FT NMR (for a review see Freeman and Kupce, 2003 or Kupce et al., 2003). In the present context, 'multi-dimensional' means that several nuclear spins are correlated and frequency labeled in the same spectrum. As a consequence, the overall experimental time is no longer dictated by resolution considerations, but only by the intrinsic sensitivity of the experiment under a given set of experimental conditions. Using modern high-field spectrometers, eventually equipped with a cryogenic probe, experimental times of several minutes up to a few hours are often sufficient, to record correlation spectra of isotope ($^{13}$C, $^{15}$N, $^{2}$H)-labeled proteins with acceptable signal to noise. This corresponds to the acquisition time required for a standard two-dimensional (2D) FT-NMR spectrum.

Recently, we have demonstrated that sequential resonance assignment is obtained from a set of 2D $^{1}$H-$^{15}$N-HSQC-like spectra (Bersch et al., 2003) where the chemical shifts of an additional nuclear spin X ($C^{\alpha}$, $C^{\beta}$, $H^{\alpha}$) are frequency-labeled together with the $^{15}$N spins. This results in zero-quantum (ZQ)- and double-quantum (DQ)-like spectra in the indirect dimension, with peak positions at $\omega_N-\omega_X$ and $\omega_N+\omega_X$, respectively. This technique has become known as reduced dimensionality spectroscopy (Szyperski et al., 1993b). The separation of the ZQ and DQ peaks in two sub-

*To whom correspondence should be addressed. E-mail: Bernhard.Brutscher@ibs.fr

spectra was first proposed by Brutscher et al. (1995b), and its generalization to the simultaneous labeling of $n$ ($n \geq 2$) chemical shifts in the same dimension has now been named GFT-NMR (Kim and Szyperski, 2003). The 2D approach is especially appealing for relatively small (< about 100 residues) $^{13}$C,$^{15}$N-labelled proteins with a well resolved $^{1}$H-$^{15}$N correlation spectrum, where the whole set of experiments required for backbone resonance assignment can be recorded in typically less than one day. For larger molecules with an increasing number of correlation peaks or for molecules with low resonance dispersion, it becomes more and more difficult to unambiguously assemble the ZQ and DQ peak pairs, providing the H-N-X frequency information of a standard 3D HNX correlation peak. Here we present a simple solution to this problem, which uses additional limited Hadamard-type sampling of the CO spectrum to simplify the 2D H-N-X correlation maps. The new approach is demonstrated on a $^{13}$C,$^{15}$N, and 77% $^{2}$H-labelled 167-residue fragment of the *Escherichia coli* sulfite reductase α-subunit (SiR-FP18) (Champier et al., 2002). Four sub-spectra are created by the Hadamard transformation, corresponding each to the spectrum of a small protein (< 60 residues), which can be analyzed independently. Hadamard CO frequency labeling can be easily added to all intra-residue and sequential correlation experiments presented previously (Bersch et al., 2003) by inserting appropriate CO inversion pulses in the sequence. Here we demonstrate that a set of CO-Hadamard-encoded intra-residue and sequential 2D H-N-CA, H-N-CB and H-N-CO correlation spectra of SiR-FP18 can be recorded with reasonably high signal to noise ratio in an overall experimental time of less than 1 day.

*Hadamard frequency-domain NMR*

Hadamard spectroscopy divides the spectrum in N parts, and a binary encoding scheme is used consisting in a series of 'plus' and 'minus' signs. Experimentally, the 'minus' sign is realized by selective inversion of the corresponding frequency band, which changes the sign of the final NMR signal. N spectra are recorded with sign encoding according to a Hadamard matrix (Hadamard, 1893). The signals corresponding to the different frequency bands are then separated by a Hadamard transformation. Hadamard-type frequency labeling disperses the NMR signals along an additional dimension. Contrary to standard time-domain FT NMR, the peak shape in this Hadamard dimension is not Lorentzian (or Gaussian), but the peak width is (generally) limited to a single point. Hadamard matrices exist for orders $N = 2^n$ or $N = 4n$ ($n = 1, 2, 3, 4,\ldots$). Therefore, the Hadamard frequency domain size can be kept as small as $N = 2$, 4, 8, 12, ... , depending on the spectral complexity and the available spectrometer time. In the simplest case, a Hadamard matrix of order 2, the experiment is recorded twice with and without inversion of a specific frequency band. Here we will focus on a Hadamard transformation of order 4 ($H_4$), where 4 experiments need to be recorded according to the following sign encoding:

| Frequency band: | A | B | C | D |
|---|---|---|---|---|
| $H_4$ – Experiment (1): | + | + | + | + |
| $H_4$ – Experiment (2): | + | + | − | − |
| $H_4$ – Experiment (3): | + | − | + | − |
| $H_4$ – Experiment (4): | + | − | − | + |

Appropriate linear combination of the four experiments separates the sub-spectra A, B, C and D. Note that there is no need of equal band widths, and that spectral regions not affected by any inversion pulse are part of the A band.

It has been suggested that Hadamard spectroscopy will become useful for application to proteins in the context of protein folding or binding studies, where only a few specific molecular sites need to be monitored (Kupce and Freeman, 2003). In this case, Hadamard encoding provides an important time advantage with respect to FT NMR for recording multi-dimensional experiments, as only the selected resonance frequencies need to be irradiated by selective pulses, each covering a small bandwidth of typically 50 Hz. Here, we are interested in the complete protein spectrum of a nuclear species, e.g., $^{13}$CO, with almost no frequency gaps. Band-selective (instead of frequency-selective) Hadamard CO encoding (CO-$H_N$) is used to simplify the 2D $^{1}$H-$^{15}$N correlation maps by spreading the peaks along the additional Hadamard dimension. Examples of 2D HN(CO-$H_4$) spectra of SiR-FP18 recorded with the pulse sequence of Figure 3a are shown in Figures 1c–f. These 2D planes can be understood as projections over different frequency bands along the CO dimension of a standard 3D HNCO spectrum. The corresponding 2D HN(CO) plane recorded without additional Hadamard CO-frequency labeling in the same experimental time is shown in Figure 1b. Clearly, spectral complexity is

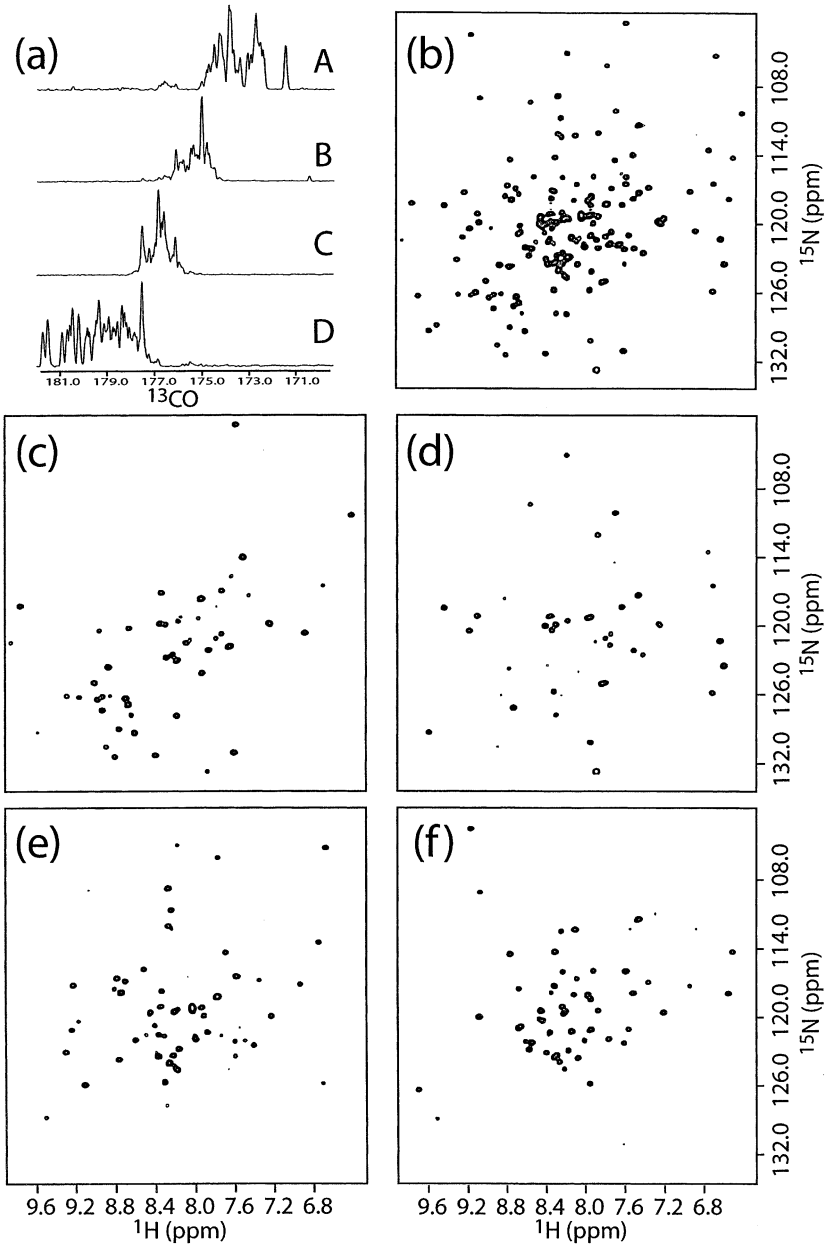


*Figure 1.* Hadamard CO-$H_4$ labeling applied to a sample of $^{13}C$, $^{15}N$ and 77% $^{2}H$-labled SiR-FP18. All spectra were recorded at 600 MHz $^{1}H$ frequency and 30 °C sample temperature. (a) Shadow projections along the CO dimension of 2D H(N)(CO-$H_4$)CO spectra recorded with the pulse sequence of Figure 3a with $t_1 = 0$ and $\lambda = 1$. (b) Reference $^{1}H$-$^{15}N$ correlation spectrum recorded with the pulse sequence of Figure 3a with $t'_1 = 0$ and no Hadamard CO-labeling. Spectra acquired with additional CO-$H_4$ labeling are shown for the A, B, C, and D-bands in (c), (d), (e), and (f), respectively. 2D data sets of 512 × 55 complex points were recorded for spectral widths of 9000 Hz ($^{1}H$) × 2000Hz ($^{15}N$). The total acquisition time for spectra (c–f) is identical to the time for spectrum (b). Mirror-image linear prediction (Zhu and Bax, 1990) was applied prior to Fourier transformation. All 2D spectra are plotted at the same contour levels.

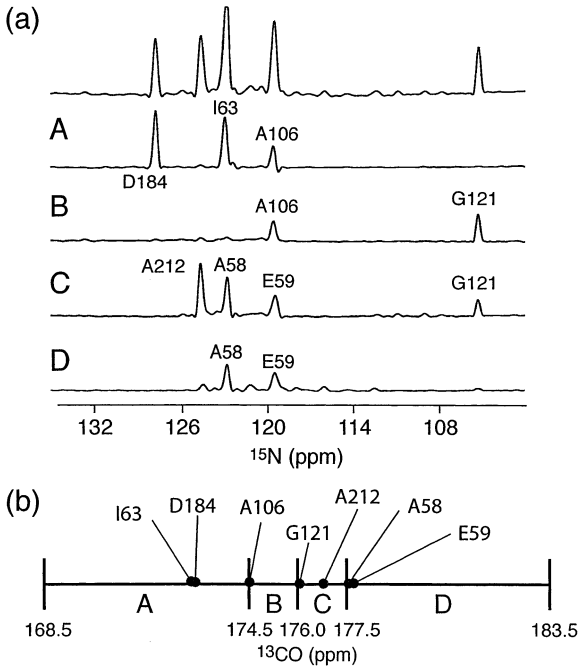


*Figure 2.* 1D traces extracted at 8.20 ppm $^{1}$H frequency from the 2D spectra of Figures 1b–f (from the top to the bottom). The corresponding residue number annotates the observed signals. Peaks, which are observed in two different sub-spectra, correspond to residues with a preceding carbonyl resonating at a band border. A schematic representation of the four CO frequency bands A–D is shown in (b). Residues observed in spectrum (a) are placed according to their CO($i-1$) frequency.

significantly reduced by this approach. A total of 47, 37, 53, and 50 correlation peaks are counted in the spectra of Figures 1c–f, respectively. All sub-spectra are well dispersed, indicating that backbone resonance assignment of this protein can be achieved using the previously proposed 2D-based assignment strategy (Bersch et al., 2003) with additional CO-$H_4$ labeling.

Experimentally, CO-$H_4$ encoding was realized by dividing the CO spectrum in four bands of unequal width, as illustrated in Figure 2b. Because the peak density increases towards the spectral center, the choice of narrower central bands ensures that a similar number of carbonyl sites are excited for each frequency band. Band-selective pulses were applied with an IBURP-2 profile (Geen and Freeman, 1991), using a linear phase ramp to shift the irradiation frequency to the center of an individual band. A single inversion pulse was used for experiments (2) and (4), with the irradiation frequency set to the center of the C–D, or B–C bands, respectively. The two inversion pulses required for experiment (3) were combined by vector addition to a single shaped pulse (Kupce and Freeman, 1993). The performance of the CO-$H_4$ labeling using this experimental scheme can be appreciated from Figure 1a, which shows 1D shadow projections along the CO dimension of a 2D H(N)CO experiment recorded with additional CO-$H_4$ encoding. Relatively clean separation of the four frequency bands is achieved. This is illustrated in Figure 2a where 1D traces along the $^{15}$N dimension are plotted, extracted from the spectra of Figures 1b–f at an amide $^{1}$H frequency of 8.20ppm. Interestingly, the cross peaks from residues I63-A58 and A106-E59 with degenerate $H^N$ and N frequencies are separated in different sub-spectra by the CO-$H_4$ labeling, which will be helpful for many practical applications. Because of the non-ideal inversion profile of band-selective pulses, spins at the band edge are only partially inverted. As a consequence, residues with a CO resonance close to a band border give rise to cross peaks in the sub-spectra corresponding to the two neighboring bands. Examples of such residues are A106, A58, E59 and G121. For these residues, correlation peaks are detected in two different sub-spectra. A splitting of the peak into different sub-spectra is observed for about 20% of the residues of SiR-FP18. For these residues, the additional Hadamard CO-frequency encoding results in an effective signal loss of about a factor $\sqrt{2}$, if both peaks are used for the spectral analysis (see below). For the other residues (e.g., D184, A212, I63), a single correlation peak is detected, with similar intensity to the corresponding peak in the reference spectrum. This indicates that, for SiR-FP18, spin relaxation during the band-selective CO pulses does not significantly affect the sensitivity of the experiment. For larger proteins, it may become advantageous to use pulse shapes with a smaller pulse width to bandwidth product, to reduce signal loss during the band-selective CO inversion pulses. Examples of such pulse shapes are the ISNOB family (Kupce et al., 1995), which allow spin inversion of a given band in a shorter time than IBURP-2, but which have a less sharp inversion profile. The use of different pulse shapes for the inner and outer frequency bands may also provide a way for adjusting the durations of the individual pulses, in order to avoid differential spin relaxation between experiments. This will increase the efficiency of peak suppression at the Hadamard decoding stage.

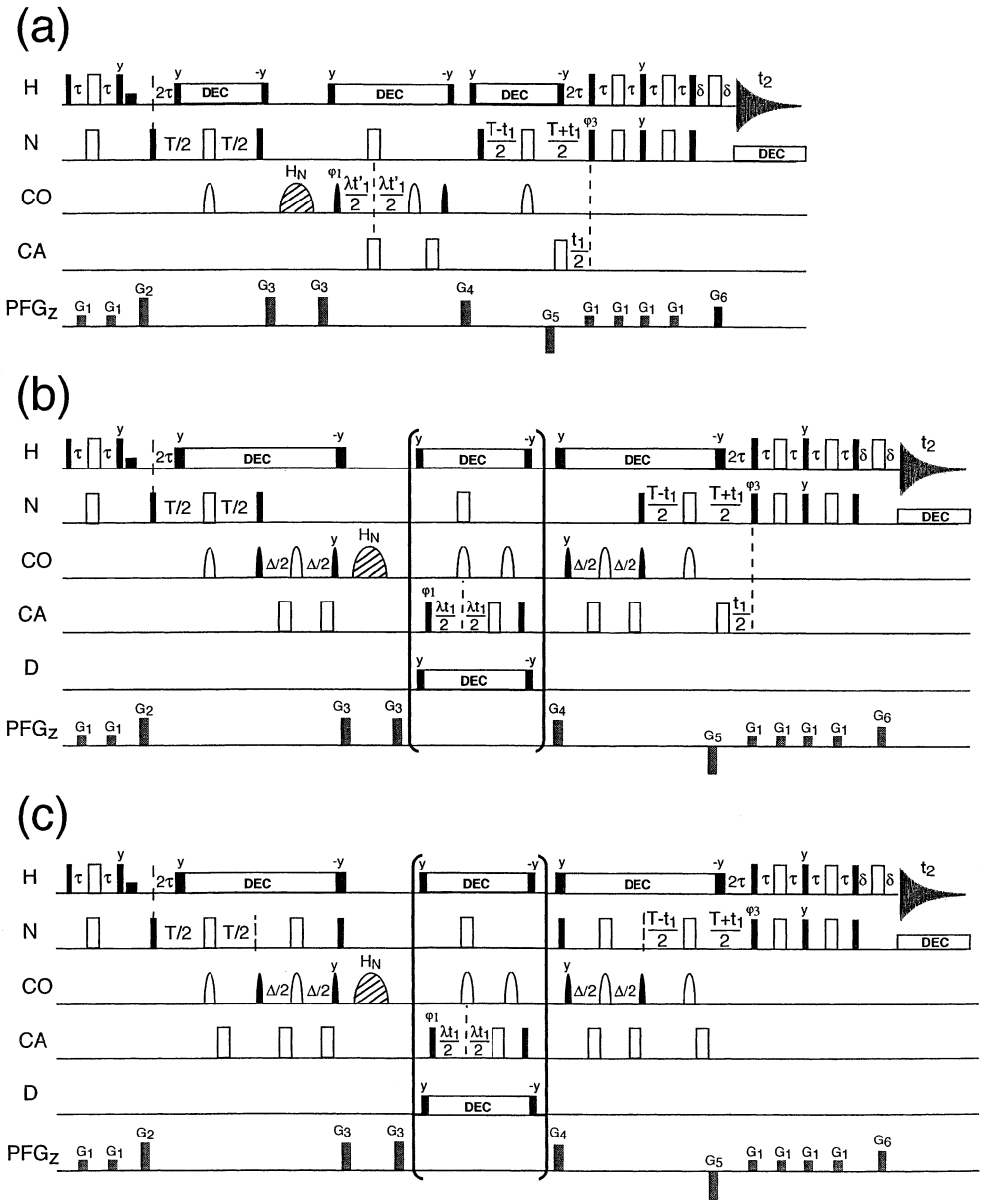


*Figure 3.* Pulse sequences for (a) sequential HN(CO-$H_N$)CO, (b) sequential HN(CO-$H_N$)CA and (c) intra-residue (CO-$H_N$)HNCA correlation experiments. All radio-frequency (rf) pulses are applied along the $x$-axis unless indicated. 90° and 180° rf pulses are represented by filled and open pulse symbols, respectively. The $^{13}C$ pulses applied to CO have the shape of the center lobe of a sin $x/x$ function, whereas the CA pulses are applied with a rectangular shape and field strength of $\Delta/\sqrt{15}$ (90°) and $\Delta/\sqrt{3}$ (180°), where $\Delta$ is the separation in Hz between the centers of the CA and CO chemical shift regions. The transfer delays are adjusted to $\tau = 1/(4J_{HN}) \cong 2.7$ ms T = $1/(2\ J_{NC'}) \cong 34$ ms, and $\Delta = 1/(2J_{C^\alpha C'}) \cong 9$ ms. Pulsed field gradients, $G_1$, $G_2$, $G_3$, $G_4$, $G_5$ and $G_6$ are applied along the $z$-axis ($PFG_z$) with a gradient strength of approximately 20 G cm$^{-1}$ and lengths ranging from 100 to 2000 μs, followed by a recovery delay of 100 μs. The relative durations of $G_5$ and $G_6$ are given by the gyromagnetic ratios of $^1H$ and $^{15}N$ as $G_5/G_6 = \gamma_H/\gamma_N$. A two-step phase cycle is used where $\varphi_1$ and the receiver phase are inverted simultaneously. Quadrature detection in the $t_1$ time-domain is obtained by repeating the experiment four times with the following phase settings: (I) $\varphi_1 = x$, $\varphi_3 = x$; (II) $\varphi_1 = y$, $\varphi_3 = x$; (III) $\varphi_1 = x$, $\varphi_3 = -x$; (IV) $\varphi_1 = y$, $\varphi_3 = -x$. In addition the sign of $G_5$ is inverted for experiments (III) and (IV). The real and imaginary parts of the ZQ and DQ coherence evolution are obtained from the four data sets as described previously (Bersch et al., 2003). For the Hadamard CO-frequency domain, N data points are recorded using appropriate band-selective inversion pulses (dashed shaped pulse on CO channel) according to a Hadamard matrix of order N. For the here presented applications I-BURP2 pulse shapes (Geen and Freeman, 1991) were used with the following irradiation frequencies (band widths): $H_4$ – Exp. (2): 180 ppm (7 ppm); $H_4$ – Exp. (3): 175.25 ppm (1.2 ppm) and 180.5 ppm (5.0 ppm); $H_4$ – Exp. (4): 176 ppm (2.5 ppm). Pulse sequence codes (Varian) and transformation protocols (Felix) can be obtained from the author upon request.

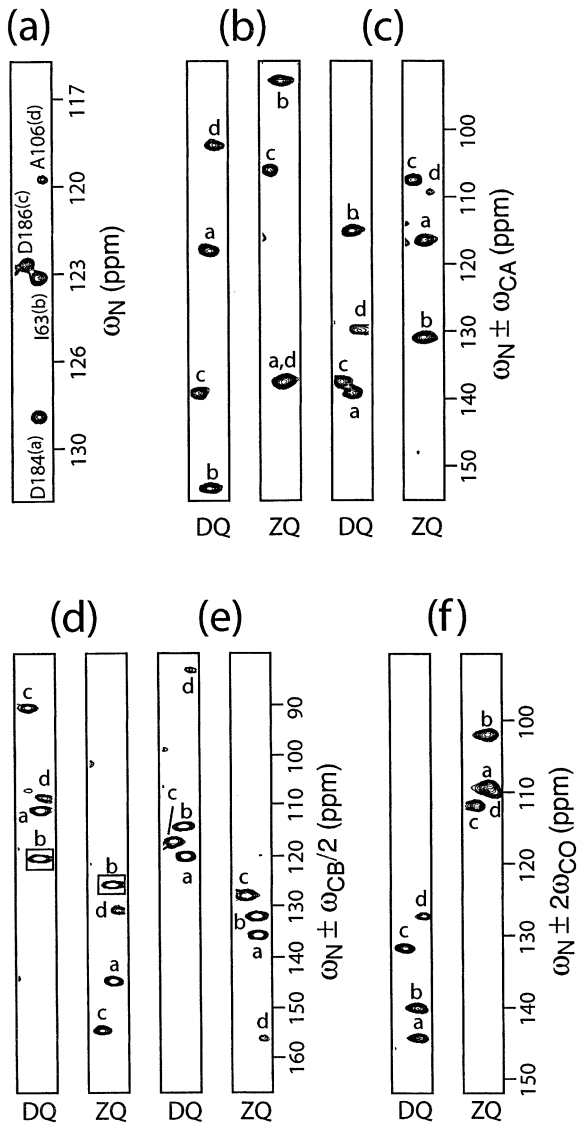


*Figure 4.* Small spectral region of A-band 2D spectra recorded on a sample of SiR-FP18 at 600 MHz $^1$H frequency: (a) HN(CO-H$_4$), (b) HN(CO-H$_4$)CA, (c) (CO-H$_4$)HNCA, (d) HN(CO-H$_4$)(CA)CB, (e) (CO-H$_4$)HN(CA)CB and (f) HN(CO-H$_4$)CO. The scaling factor ($\lambda$), spectral widths, and $t_1$ increments (ni) were set to: (a) 9000 Hz ($^1$H), 2000Hz ($^{15}$N), ni = 55; (b) and (c) 9000 Hz ($^1$H), 6000Hz (ZQ/DQ), ni = 120, $\lambda$ = 1.0; (d) and (e) 9000 Hz ($^1$H), 8000 Hz (ZQ/DQ), ni = 150, $\lambda$ = 0.5; (f) 9000 Hz ($^1$H), 4500 Hz (ZQ/DQ), ni = 100, $\lambda$ = 2.0. Acquisition times are given in the text. Correlation peaks for all four residues in this small spectral region were observed and unambiguously assigned. A negative cross peak (indicated by a box) is detected for residue I63 in the sequential HNCB correlation spectra (d), because the preceding residue is a glycine.

**Application to protein resonance assignment**

The previously proposed 2D-based sequential assignment strategy (Bersch et al., 2003) uses a set of sequential and intra-residue H-N-X correlation experiments. These uni-directional experiments are particularly well suited for low-dimensionality implementations because the maximum number of peaks per spectrum is equal to the number of non-proline residues in the peptide sequence. An interesting and general feature of these sequences is that the CO spins get polarized during the pulse sequence, although they are not frequency edited in the originally proposed experiments. In the sequential correlation experiments, spin polarization is transferred as follows:

$$\begin{aligned} H_z^i \;&\rightarrow\; 2N_z^iH_z^i \rightarrow 2N_z^iCO_z^{i-1} \\ &\rightarrow 4N_z^iCO_z^{i-1}CA_z^{i-1} \rightarrow \ldots . \end{aligned} \quad (1)$$

For the intra-residue correlation experiments (Brutscher, 2002) one obtains a very similar correlation pathway:

$$H_z^i \rightarrow 2N_z^iH_z^i \rightarrow 4N_z^iCO_z^{i-1}CA_z^i \rightarrow \ldots . \quad (2)$$

The arrow at the end indicates eventual further polarization transfer to CB or HA. In both types of experiments the carbonyl spin of the preceding residue is polarized after the initial transfer steps. This may be exploited by additional time-domain CO frequency editing, as proposed in the past (Brutscher et al., 1995; Szyperski et al., 1995; Brutscher, 2002), or, as demonstrated here, by Hadamard-type frequency-domain encoding of the CO chemical shifts. Pulse sequences for sequential HN(CO-H$_N$)CA and intra-residue (CO-H$_N$)HNCA are shown in Figures 3b and 3c, respectively. Differences with respect to previously presented sequences (Bersch et al., 2003) are the addition of a band-selective CO pulse for the Hadamard frequency labeling, and of deuterium decoupling during CA transverse coherence evolution, for application to partially or perdeuterated molecules. (CO-H$_N$)-encoded intra-residue and sequential H-N-CB or H-N-HA correlation experiments are easily derived from these pulse sequences by replacing the central part of the sequence by the appropriate transfer and labeling block, as shown in Bersch et al. (2003).

2D HN(CO-H$_4$), HN(CO-H$_4$)CO, HN(CO-H$_4$)CA, HN(CO-H$_4$)(CA)CB, (CO-H$_4$)HNCA, and (CO-H$_4$) HN(CA)CB correlation spectra were recorded on a 1.4 mM sample of $^{13}$C,$^{15}$N and 77% $^2$H-labeled SiR-FP18 on a Varian INOVA 600 spectrometer

equipped with a standard triple-resonance probe at a sample temperature of 30 °C. The individual acquisition times were adjusted to account for the intrinsic sensitivity of the different experiments, and set to 30 min for HN(CO-$H_4$), 50 min for HN(CO-$H_4$)CO, 1 h for HN(CO-$H_4$)CA, 2 h for (CO-$H_4$)HNCA, 5 h for HN(CO-$H_4$)(CA)CB, and 10 h for (CO-$H_4$)HN(CA)CB. 8 sub-spectra are obtained per experiment corresponding to ZQ- and DQ-type correlation spectra for each of the four CO-frequency bands (A, B, C and D). Strip plots extracted from the A-band spectra are shown in Figure 4. Four correlation peaks are observed in the selected spectral region. The ZQ and DQ peak pairs are assigned by exploiting their symmetry with respect to a 'central peak', detected in the corresponding A-band HN(CO-$H_4$) spectrum (Figure 4a). This procedure also allows the detection of accidental peak overlaps, as observed in the ZQ spectrum of Figure 4b for the correlation peaks of residues D186 and A106. The ZQ and DQ sub-spectra for a given CO-frequency band can be analyzed independently from the spectra recorded for the other bands. As spectral complexity is that of a small ($< 60$ residues) protein, spectral analysis is straightforward. For SiR-FP18, all expected peaks were observed and unambiguously assigned from these spectra. The signal to noise ratio is sufficient to detect the ZQ and DQ peaks for residues with a CO frequency at the border of two bands, e.g., A106 is detected in the A- and B-band spectra (see Figure 2a). Note that for these peaks, the redundant information obtained from two sets of spectra can be used to increase the precision of the measured ZQ and DQ peak positions. This partially compensates for the signal loss due to the peak splitting in two sub-spectra.

A simple protocol is used to extract and combine the chemical shift information of the different 2D spectra: First, a peak picking of all spectra is performed. To simplify further analysis, it is helpful to use the same peak number for 'central peaks' with identical $H^N$ and N frequencies, and detected in different HN(CO-$H_4$) spectra. In a second step, the H-N-X frequency information is extracted from the ZQ, DQ and central peak lists for each band and experiment by applying the symmetry criterion. The different experiments are than combined to yield the frequency information of small protein segments of the form:

$$\mathrm{CB}(i-1) - \mathrm{CA}(i-1) - \mathrm{CO}(i-1) - \mathrm{HN}(i) - \mathrm{N}(i) - \mathrm{CA}(i) - \mathrm{CB}(i). \quad (3)$$

In a last step redundant segments from different CO-bands are combined to a single one, and the list of segments from all bands provides the input for sequential assignment using standard assignment protocols. Manipulation of peak picking lists is performed using a suite of c-programs, which are available from the author upon request. Almost complete assignment for all protein segments, as compared to our previous assignment work (Sibille et al., 2001), was obtained. The whole set of 2D spectra was recorded in only about 20 h, whereas the initial assignment based on 3D and MQ-3D experiments required about 2 weeks of data collection.

The protein segments (Equation 3) can be further extended to the HA($i-1$) and HA($i$) nuclei using the same (CO-$H_N$)-encoded 2D approach by recording the corresponding (CO-$H_N$)HN(CA)HA and HN(CO-$H_N$)(CA)HA experiments on a protonated sample of the protein. The experiments are easily derived from the sequences of Figures 3b and 3c by replacing the central pulse sequence part by the appropriate building block (Bersch et al., 2003). Alternatively, the assignment can be complemented by a standard 3D HN(CA)CO experiment to yield the chemical shift information of the CO(i) nuclei.

## Conclusions

A simple and general method is presented which simplifies the spectra of standard multi-dimensional correlation experiments by introducing additional Hadamard-type frequency labeling. It has been shown that 4-step Hadamard CO-frequency labeling allows recording of $^1$H-$^{15}$N correlation maps of a larger protein with the spectral complexity of a four-times smaller one, while increasing the minimal experimental time by only a factor of 4. One can imagine that the high resolution obtained in these 2D correlation spectra may improve many existing NMR techniques or extend their field of applicability. Examples are the study of protein dynamics by spin relaxation measurements, the study of molecular interfaces by chemical shift mapping, or the measurement of spin–spin coupling constants. Here, we have demonstrated that sequential backbone resonance assignment of a 167-residue protein is obtained from a set of 2D reduced-dimensionality experiments, recorded in an overall experimental time of only about 1 day. This 2D assignment strategy, initially proposed for application to relatively small proteins, can now

be used for larger molecular systems, or molecules, e.g. partially unfolded proteins, with highly degenerate resonance frequencies. In many cases, this will result in a significant time advantage with respect to standard 3D or 4D-based methods. Short acquisition times are not only important in the context of high-throughput NMR studies but also in the case of unstable proteins with a limited life time. Band-selective Hadamard frequency encoding can be applied to any multi-dimensional NMR experiment to reduce spectral complexity without complete frequency labeling of an additional nuclear spin. It is expected that the combination of Hadamard-frequency-domain and FT- or GFT-time-domain NMR spectroscopy will become widespread in bio-molecular NMR.

## Acknowledgements

This work was supported by the Commissariat à l'Energie Atomique and the Centre National de la Recherche Scientifique. The author thanks N. Sibille, B. Bersch and J. Covès for the preparation of the labeled protein sample.

## References

Bersch, B., Rossy, E., Covès, J. and Brutscher, B. (2003) *J. Biomol. NMR*, **27**, 57–67.

Brutscher, B. (2002) *J. Magn. Reson.*, **156**, 155–159.

Brutscher, B., Cordier, F., Simorre, J.-P., Caffrey, M. and Marion D. (1995a) *J. Biomol. NMR*, **5**, 202–206.

Brutscher, B., Morelle, N., Cordier, F. and Marion D. (1995b) *J. Magn. Reson.*, **B109**, 238–242.

Brutscher, B., Simorre, J.-P., Caffrey, M. and Marion D. (1994) *J. Magn. Reson.*, **B105**, 77–82.

Champier, L., Sibille, N., Bersch, B., Brutscher, B., Blackledge, M. and Covès, J. (2002) *Biochemistry*, **41**, 3770–3780.

Chen, J., De Angelis, A.A., Mandelshtam, V.A. and Shaka, A.J. (2003) *J. Magn. Reson.*, **161**, 74–89.

Chen, J., Mandelshtam, V.A. and Shaka, A.J. (2000) *J. Magn. Reson.*, **146**, 363–368.

Ding, K. and Gronenborn, A. (2002) *J. Magn. Reson.,* **156**, 262–268.

Freeman, R. and Kupce, E. (2003) *J. Biomol. NMR*, **27**, 101–113.

Frydman, L., Lupulescu, A. and Scherf, T. (2003) *J. Am. Chem. Soc.*, **125**, 9204–9217.

Frydman, L., Scherf, T. and Lupulescu, A. (2002) *Proc. Natl. Acad. Sci. USA*, **99**, 15859–15862.

Geen, H. and Freeman, R. (1991) *J. Magn. Reson.*, **93**, 93–141.

Hadamard, J. (1893) *Bull. Sci. Math.*, **17**, 240–248.

Kim, S. and Szyperski, T. (2003) *J. Am. Chem. Soc.*, **125**, 1385–1393.

Kozminski, W. and Zhukov, I. (2003) *J. Biomol. NMR*, **26**, 157–166.

Kupce, E. and Freeman, R. (1993) *J. Magn. Reson.*, **A105**, 234–238.

Kupce, E. and Freeman, R. (2003a) *J. Magn. Reson.*, **162**, 158–165.

Kupce, E. and Freeman, R. (2003b) *J. Magn. Reson.*, **162**, 300–310.

Kupce, E. and Freeman, R. (2003c) *J. Magn. Reson.*, **163**, 56–63.

Kupce, E., Boyd, J. and Campbel, I.D. (1995) *J. Magn. Reson.*, **B106**, 300–303.

Kupce, E., Nishida, T. and Freeman, R. (2003d) *Prog. NMR Spectrosc.*, **42**, 95–122.

Mandelshtam, V.A. (2001) *Prog. NMR Spectrosc.*, **38**, 159–196.

Sibille, N., Covès, J., Marion, D., Bersch, B. and Brutscher, B. (2001) *J. Biomol. NMR*, **21**, 71–72.

Simorre, J.-P., Brutscher, B., Caffrey, M. and Marion D. (1994) *J. Biomol. NMR*, **4**, 325–333.

Szyperski, T., Banecki, B., Braun, D. and Glaser R. W. (1998) *J. Biomol. NMR*, **11**, 387–405.

Szyperski, T., Braun, D., Banecki, B. and Wüthrich K. (1996) *J. Am. Chem. Soc.*, **118**, 8146–8147.

Szyperski, T., Braun, D., Fernandez, C., Bartels, C. and Wüthrich, K. (1995) *J. Magn. Reson.*, **B108**, 197–203.

Szyperski, T., Pellecchia, M. and Wüthrich K. (1994) *J. Magn. Reson.*, **B105**, 188–191.

Szyperski, T., Wider, G., Bushweller, J.H. and Wüthrich, K. (1993a) *J. Biomol. NMR*, **3**, 127–132.

Szyperski, T., Wider, G., Bushweller, J.H. and Wüthrich, K. (1993b) *J. Am. Chem. Soc.*, **115**, 9307–9308.

Szyperski, T., Yeh, D.C., Sukumaran, D.K., Moseley, H.N.B. and Montelione G.T. (2002) *Proc. Natl. Acad. Sci. USA*, **99**, 8009–8014.

Zhu, G. and Bax, A. (1990) *J. Magn. Reson.* **B90**, 405–410.